Available online at www.sciencedirect.com

ScienceDirect

Procedia Structural Integrity 22 (2019) 10–16

Structural Integrity Procedia

www.elsevier.com/locate/procedia

First International Symposium on Risk and Safety of Complex Structures and Components

Fatigue behaviour of maraging steel samples produced by SLM under constant and variable amplitude loading

R. Branco[a]*, J. Silva[a], J. Martins Ferreira[a], J.D. Costa[a], C. Capela[a,b], F. Berto[c] L. Santos[a], F.V. Antunes[a]

[a]*CEMMPRE, Department of Mechanical Engineering, University of Coimbra, Coimbra, 3030-788 Coimbra, Portugal*

[b]*Department of Mechanical Engineering, ESTG, Polytechnic Institute of Leiria, Morro do Lena - Alto Vieiro, Leiria, 2411-901 Leiria, Portugal*

[c]*Department of Mechanical and Industrial Engineering, NTNU, 7491 Trondheim, Norway*

Abstract

This paper addresses the fatigue behaviour of AISI 18Ni300 samples manufactured by selective laser melting under both constant- and variable-amplitude loading. The fatigue campaign encompasses a series of low-cycle strain-controlled fatigue tests performed under fully-reversed conditions at various strain amplitudes, and a series of high-cycle stress-controlled fatigue tests performed under pulsating conditions at various stress ranges considering both constant- and variable-amplitude loading spectra. Fatigue life predictions are performed on the basis of the SWT parameter along with the Miner's law. This approach has demonstrated to be sufficiently reliable to predict the lifetime expectancy in maraging steel samples produced by selective laser melting.

Keywords: AISI 18Ni300; maraging steel; selective laser melting; variable-amplitude loadig, fatigue life prediction

* Corresponding author. Tel.: +351-239-790-700; fax: +351-239-403-407.
E-mail address: ricardo.branco@dem.uc.pt

10.1016/j.prostr.2020.01.002

1. Introduction

Nomenclature

AM	additive manufacturing
b	fatigue strength exponent
c	fatigue ductility exponent
CA	constant-amplitude loading
$d\varepsilon/dt$	strain rate
LCF	low-cycle fatigue
N_f	number of cycles to failure
N_p	predicted life
N_e	experimental life
R_ε	strain ratio
R_σ	stress ratio
SLM	selective laser melting
SWT	Smith-Watson-Topper parameter
VA	variable-amplitude loading
$\Delta\sigma$	stress range
σ_f'	fatigue strength coefficient
ε_f'	fatigue ductility coefficient
ΔW_p	plastic strain energy density
$\Delta\varepsilon/2$	strain amplitude

Driven by a significant number of technical benefits, additive manufacturing applications are rapidly expanding in various strategic industries, such as automotive, aeronautical, aerospace, biomedical, electronic, and moulds, among others [1]. Although these new technologies have brought new perspectives for fabrication, either in terms of shape solutions or in terms of assembly possibilities, additive manufacturing processes are unequivocally complex. Firstly, there are a vast number of techniques; secondly, microstructure and mechanical properties are parameter-sensitive; and, thirdly, mechanical properties can be drastically affected by the fabrication methodology [2].

Within the laser-based additive manufacturing techniques, selective laser melting is one of the most promising methodologies for metal processing. SLM is able to produce, in an industrial environment, physical objects, directly from three-dimensional computer models, in a layer-by-layer fashion. SLM products are prone to various anomalies, namely porosities, lack of fusion, inclusions, micro-cracking, shrinkage, excessive roughness at surface, increasing the uncertainty in structural properties due to the randomly dispersed defects and heterogeneities [3-5]. Therefore, the full understanding of the long-term structural integrity of such products is pivotal to develop durable and reliable engineering products. Nevertheless, so far, the triangular relationships between process parameters, final mechanical properties, and fatigue response, is far from optimum. Moreover, in SLM-produced parts, the effect of the loading history on the lifetime expectancy, particularly under complex loading scenarios, remains unclear.

The critical components of the above-mentioned high-value added industries are often subjected to variable-amplitude fatigue spectra. In this context, the analysis of the cumulative damage plays an important role on fatigue lifetime assessment. Particularly in the case of maraging steel samples produced by selective laser melting, studies dealing with variable-amplitude loading scenarios are scarce [6]. Research has mainly dealt with the influence of the processing and post-processing parameters on mechanical properties [7,8]. Therefore, the paper aims at studying the fatigue behaviour of AISI 18Ni300 samples produced by selective laser melting undergoing variable-amplitude loading. The fatigue test campaign includes: (i) strain-controlled axial fatigue tests performed under fully-reversed conditions at various strain amplitudes; and (ii) high-cycle stress-controlled axial fatigue tests conducted at pulsating conditions with both constant- and variable-amplitude loading spectra. Fatigue lifetime predictions are determined via the SWT parameter, defined for this maraging steel from the mid-life circuits collected in the low-cycle fatigue tests. After fatigue testing, fractography analysis is carried out to identify the main fatigue damage mechanisms.

2. Experimental procedure

The material used in this study an AISI 18Ni300 maraging steel produced by selective laser melting using a Concept Laser M3 linear printing system. The main mechanical properties are summarised in Table 1. Samples were deposited vertically in the direction of load application with a sintering scan of 200 m/s. After production, all samples were machined and polished to a scratch-free condition. Figure 1 shows the metallography in the longitudinal section of the sample. Microstructure is rather coherent and is essentially formed by elongated grains with about 150 μm long and 30–35 μm width. It is also possible to observe a considerable level of small porosities, as well as martensitic needles identified by the dashed-line circles.

The test program included low-cycle strain-controlled and high-cycle stress-controlled fatigue tests. Low-cycle fatigue tests (LCF) were conducted under fully-reversed strain-controlled conditions ($R_\varepsilon = -1$) with sinusoidal waves and a constant strain rate ($d\varepsilon/dt = 8\times10^{-3}$ s) using smooth specimens with 19mm-long and 6mm-diameter cylindrical gauge sections. Strain amplitudes ($\Delta\varepsilon/2$) were defined in the range 0.3 to 1.0%. The stress-strain response was acquired via an axial extensometer clamped directly to the gauge section. Tests were interrupted when the specimens reached the total failure.

Constant- and variable-amplitude axial fatigue tests were performed in load control mode, under pulsating conditions ($R_\sigma = 0$), with frequencies between 15 and 20 Hz, and using sinusoidal waves. In the constant-amplitude tests, stress range varied between 300 and 700 MPa. In the variable-amplitude tests, the block load spectra included three stress levels, applied 1000 cycles each (see Figure 2) with maximum stress ranges in the interval 450 to 700 MPa. The samples used in the high-cycle fatigue campaign had a gauge section with a length of 30 mm and a diameter of 4 mm. Tests were interrupted when the specimens reached the total failure.

Fig.1. Optical micrograph in the longitudinal direction (sample etched with Picral).

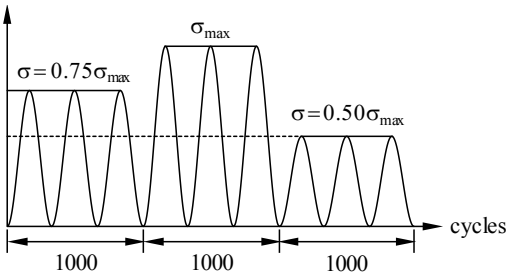

Fig. 2. Block load spectrum of the variable-amplitude high-cycle fatigue test program.

Table 1. Mechanical properties of AISI 18NI300 maraging steel produced by SLM [9].

Tensile Strength (MPa)	Yield Strength (MPa)	Young's Modulus (GPa)	Density (g/m^3)	Porosity (%)
1147	910	168	7.42	0.74

3. Results and discussion

Figure 3 shows the stress-strain response of the AISI 18Ni300 sample produced by selective laser melting in the low-cycle fatigue test at a strain amplitude ($\Delta\varepsilon/2$) of 1%. For the sake of clarity, the second and mid-life circuits are plotted in red and blue, respectively. This steel shows a cyclic strain-softening behavior throughout the entire lifetime, since the peak tensile stress decreases with the increasing number of loading cycles. This transient response occurs only at the first few cycles. After that, the stress-strain response stabilises and, only in a final stage of the test, for life ratios (N/N_f) greater than 90%, the tensile stress drops rapidly culminating in the total failure [9].

The area of the hysteresis loops, which represents the plastic strain energy per cycle, can be regarded as a main contribution to the fatigue damage process taking place in each cycle. Although there are changes during the test, this energy is almost constant. This conclusion can be clearly observed in Figure 4 which plots the plastic strain energy

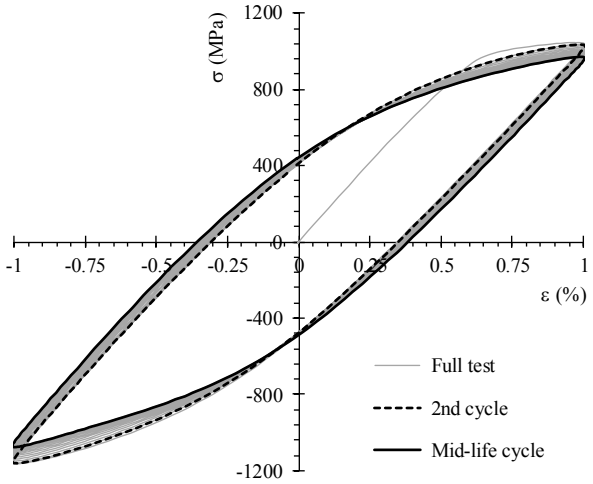

Fig. 3. Stress-strain response in a low-cycle fatigue test at $\Delta\varepsilon/2$=1.0%.

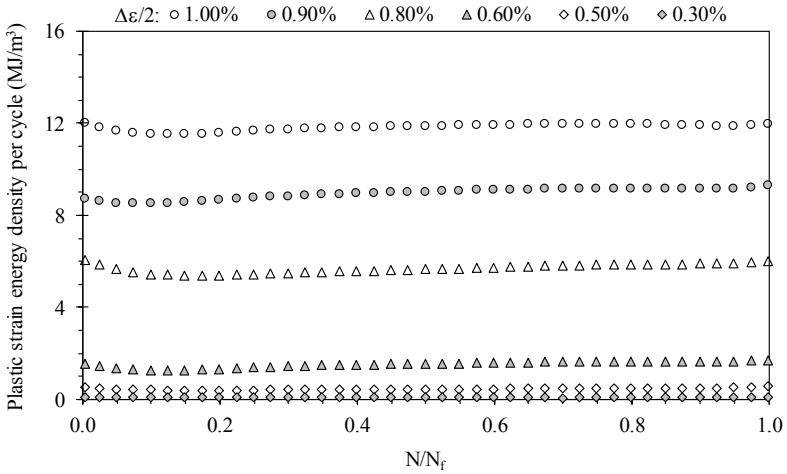

Fig. 4. Evolution of plastic strain energy density with dimensionless life for various strain amplitudes.

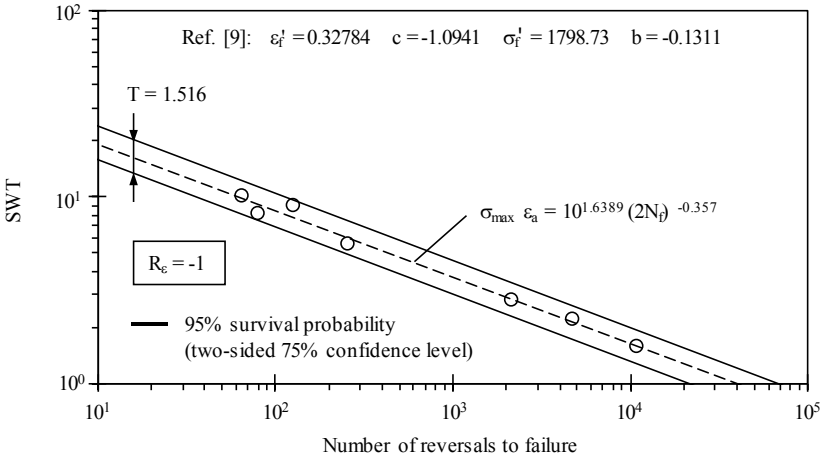

Fig. 5. SWT parameter versus number of reversals to failure defined from the mid-life hysteresis loops of the LCF tests.

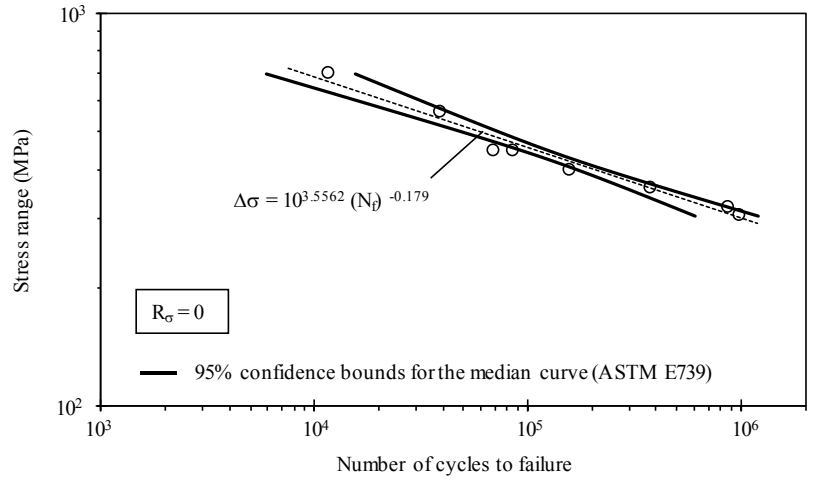

Fig. 6. Stress range versus fatigue life for the samples tested under constant-amplitude stress-controlled conditions.

density against the life ratio for various strain amplitudes. Regardless of the $\Delta\varepsilon/2$ value, ΔW_p remains nearly constant throughout the test, particularly for life ratios between 10 and 90%. In the first cycles, the plastic strain energy density slightly decreases, evidence of a cyclic strain-softening behaviour, then attains a stabilised response and, at a final stage of the test, there is a rapid decay of the ΔW_p value until total failure occurs.

The plastic strain energy density and the fatigue life for the AISI 18Ni300 produced by selective laser melting, as in other high-strength steels can be correlated, in log-log scale, by a linear relationship [9]. Nevertheless, at lower strain amplitudes, the plastic strain energy density is difficult to measure. Moreover, this damage parameter is unsensitive to the mean stress, which is another disadvantage. Within the various methods to deal with the mean stress effect, the SWT approach has been successfully applied in different contexts [10-12]. This damage parameter, although not formally defined as such, can be recognized as an energy-based parameter. In this particular case, as exhibited in Figure 5, there is an excellent correlation between both variables. This fact suggests that the SWT parameter can be used to account for the fatigue damage for this material. The values of the SWT parameter were calculated from the mid-life circuits recorded for the various strain amplitude of the tests performed under strain-controlled conditions. The mean curve (dashed line) was fitted to the experimental data with a high correlation coefficient (r = 0.993). The upper and lower bounds were drawn for a 95% survival probability calculated from the mean value assuming two-sided confidence levels equal to 75%. The scatter band index (T) is equal to 1.516.

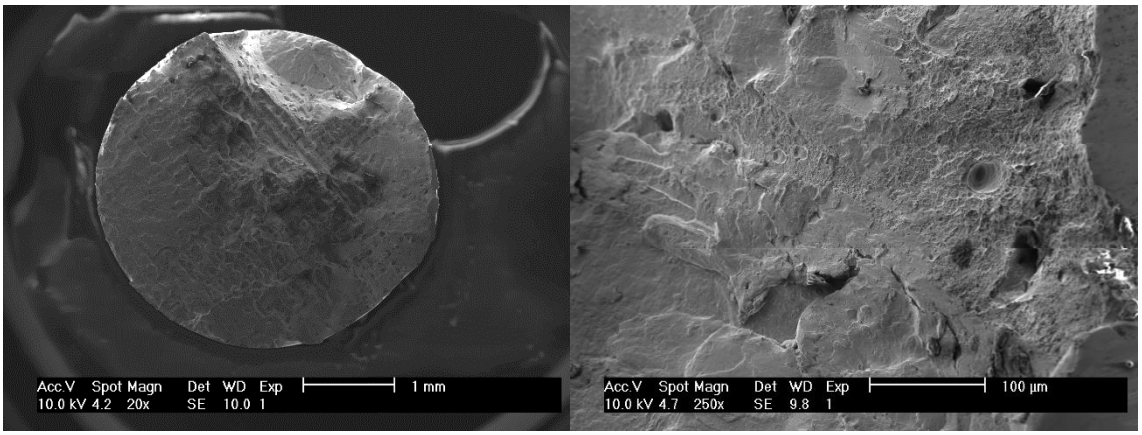

Fig. 7. SEM images of fracture surfaces of a sample tested under stress-controlled conditions.

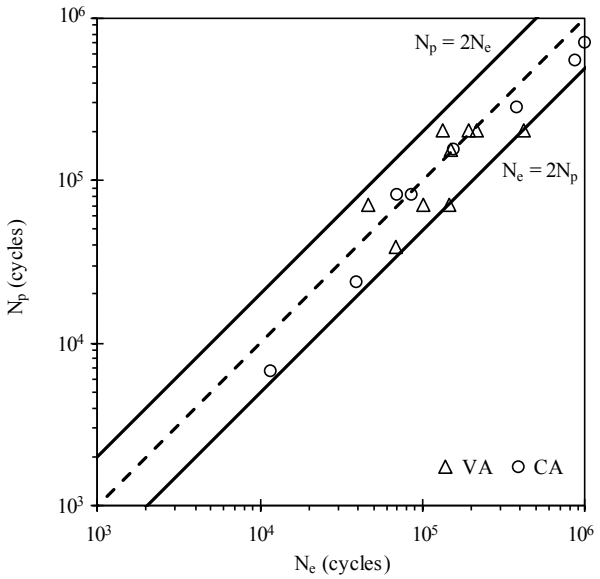

Fig. 8. Comparison of experimental versus predicted lives of samples subjected to constant- and variable-amplitude loading.

The fatigue results of the constant-amplitude axial fatigue tests, represented in terms of stress range versus number of cycles, are exhibited in Figure 6. In general, experimental results are quite close to the fitted S-N curve. This closeness is reinforced by the high correlation coefficient ($r = 0.986$). This figure also displays the 95% confidence bounds for the median curve determined following the procedure outlined in ASTM E739 standard. SEM images of fracture surfaces, as can be distinguished in Figure 7, show that cracks initiated around the surface and, then, propagated through the cross-section (Figure 7(a)). Mixed failure mode was observed: intergranular fracture between the deposited layers and transgranular crack propagation with traces of significant plastic deformation (Figure 7(b)).

Figure 8 compares the experimental fatigue lives with those predicted on the basis of the SWT relationship defined for this material for constant-amplitude stress-controlled tests. Overall, as can be seen, the SWT damage parameter is able to predict the lifetime in the AISI 18Ni300 maraging steel produced by SLM. Regarding the variable-amplitude axial fatigue tests, fatigue damage accumulation has been computed by the Miner's law. The damage accumulation induced by each loading block was estimated via the SWT relationship as the ratio of the applied number of cycles to the fatigue lifetime associated with this loading block. Figure 8 plots the experimental lives against the predicted values for the variable-amplitude fatigue tests performed here. Once again, as for the constant-amplitude loading,

there is a very good correlation in the entire range, with all the points within scatter bands of two (i.e. $N_p = 2N_e$ and $N_e = 2N_p$) which is satisfactory. Furthermore, in general, predictions are conservative, which is also interesting. Therefore, these results show that the proposed methodology can be successfully applied to analyse the fatigue lifetime in additively manufactured samples undergoing variable amplitude loading histories.

4. Conclusions

The present paper dealt with the fatigue behaviour of AISI 18Ni300 samples produced by selective laser melting subjected to constant- and variable-amplitude loading. Fatigue life predictions were carried out via the SWT parameter which was defined on the basis of the mid-life circuits recorded in the low-cycle fatigue tests. Damage accumulation was estimated using the Miner's law. The following conclusions can be drawn:

- The SWT parameter has been successfully applied in the fatigue life prediction of AISI 18Ni300 samples produced by selective laser melting subjected to constant-amplitude loading;
- The Miner's law along with the STW parameter have been successfully applied in the prediction of fatigue lifetime under variable-amplitude loading spectra of AISI 18Ni300 samples produced by selective laser melting;
- Fatigue life predictions under constant- and variable-amplitude loading agree well with the experimental results, with all the tests within a scatter band of two. Fatigue life predictions are, in general, conservative;
- SEM images revealed that crack nucleation occurs around the surface of the specimen and, then, propagate through the cross-section. A mixed intergranular-transgranular failure mode has been observed.

Acknowledgements

This work was financially supported by: Project PTDC/CTM-CTM/29101/2017 – POCI-01-0145-FEDER-029101 funded by FEDER funds through COMPETE2020 - Programa Operacional Competitividade e Internacionalização (POCI) and by national funds (PIDDAC) through FCT/MCTES.

References

1. Pinkerton, A.J, 2016. Lasers in additive manufacturing. Optics and Laser Technology 78, 25–32.
2. Fayazfar, H., Salarian, M., Rogalsky, A., Sarker, D., Russo, P., Paserin, V., Toyserkani, E., 2018. A critical review of powder-based additive manufacturing of ferrous alloys: Process parameters, microstructure and mechanical properties. Materials and Design 144, 98–128.
3. Mooney, B., Kourousis, K., Raghavendra, R., 2019. Plastic anisotropy of additively manufactured maraging steel: Influence of the build orientation and heat treatments. Additive Manufacturing 25, 19–31.
4. Wei, M., Chen, S., Xi, L., Liang, J., Liu, C., 2018. Selective laser melting of 24CrNiMo steel for brake disc: fabrication efficiency, microstructure evolution, and properties. Optics and Laser Technology 107, 99–109.
5. Razavi, S., Ferro, P., Berto, F., 2018. Fatigue assessment of Ti–6Al–4V circular notched specimens produced by selective laser melting. Metals 11(2), 284.
6. Santos, L., Ferreira, J., Silva, J., Costa, J., Capela, C., 2016. Fatigue behaviour of selective laser melting steel components. Theoretical and Applied Fracture Mechanics 85, 9–15.
7. Tan, C., Zhou, K., Ma, W., Zhang, P., Liu, M., Kuang, T., 2017. Microstructural evolution, nanoprecipitation behavior and mechanical properties of selective laser melted high-performance grade 300 maraging steel. Materials and Design 134, 23–34.
8. Croccolo, D., De Agostinis, M., Fini, S., Olmi, G., Bogojevic, N., Ciric-Kostic, S., 2018. Effects of build orientation and thickness of allowance on the fatigue behaviour of 15−5 PH stainless steel manufactured by DMLS. Fatigue & Fracture of Engineering Materials & Structures 41, 900-916.
9. Branco, R., Costa, J., Berto, F., Razavi, S., Ferreira, J., Capela, C., Santos, L., Antunes, F., 2018. Low-cycle fatigue behaviour of AISI 18Ni300 maraging steel produced by selective laser melting, Metals 8(1), 32.
10. Ince, A., 2017. A generalized mean stress correction model based on distortional strain energy. International Journal of Fatigue 104, 273–282.
11. Correia, J., Apetre, N., Attilio, A., De Jesus, A., Muñiz-Calvente, M., Calçada, R., Berto, F., Canteli, A., 2017. Generalized probabilistic model allowing for various fatigue damage variables. International Journal of Fatigue 100, 187–194.
12. Branco, R., Antunes, F.V., Martins, R.F., 2008. Modelling fatigue crack propagation in CT specimens. Fatigue and Fracture of Engineering Materials and Structures 31,452–465.